L-ferritin: A theranostic agent of natural origin for MRI visualization and treatment of breast cancer

L-ferritin: A theranostic agent of natural origin for MRI visualization and treatment of breast cancer

Valeria Bitonto 1, Diego Alberti 1, Roberto Ruiu 1, Silvio Aime 1, Simonetta Geninatti Crich 1, Juan Carlos Cutrin 2

1University of Torino, Department of Molecular Biotechnology and Health Sciences, Via Nizza 52, 10126 Torino, Italy.

2University of Torino, Department of Molecular Biotechnology and Health Sciences, Via Nizza 52, 10126 Torino, Italy. Electronic address: juancarlos.cutrin@unito.it.

Abstract

The altered regulation of iron uptake and metabolism in cancerous cells, along with the potential of this metal to cause oxidative stress and cell death, makes iron overload an attractive therapeutic strategy for cancer treatment. In this study, the selective uptake of native HoS-ferritin (Horse-Spleen Ferritin) was assessed in TS/A breast cancer cells and compared with benign cystadenoma NMuMG. The higher expression of L-ferritin receptor SCARA5 led to an enhanced uptake in TS/A that is detected by the generation of a negative contrast in the corresponding MR images. The toxicity of HoS-ferritin toward TS/A cells has been investigated in detail in vitro, showing that cellular vitality is inversely related to the amount of internalized iron content. Finally, biodistribution and therapeutic efficacy of HoS-ferritin have been shown for the first time in vivo on a orthotopic breast cancer mice model, suggesting that iron overdose delivered by the HoS-ferritin can trigger selective mechanisms of regulated cell death.

Keywords

Ferritin

Magnetic resonance imaging

Theranostic

Molecular imaging

Iron overloading

Abbreviations

CD71Cluster of Differentiation 71

ELCEndolysosomal compartment

FOVField Of View

HoS-ferritinHorse Spleen Ferritin

ICP-MSInductively Coupled Plasma Mass Spectrometry

LAMP1Lysosomal-Associated Membrane Protein 1

MRIMagnetic Resonance Imaging

MTXMatrix

NEXNumber of Excitations

PBSPhosphate-Buffered Saline

PFAParaformaldehyde

ROSReactive Oxygen Species

SCARA5Scavenger Receptor Class A Member 5

SISignal Intensity

TEEcho Time

TfR1Transferrin Receptor 1

TRRepetition Time

Background

Ferritin is the main iron storage protein found in most living organisms and is composed of 24 subunits of heavy (H)- or light (L)-chain peptides that self-assemble to form a spherical, cage-like architecture, 12 nm in external diameter with an interior cavity of 8 nm [1]. The two subunits share a similar fold and 53% sequence identity, but differ in their ability to handle iron. H-subunits contain a catalytic center (ferroxidase or oxidoreductase site) where iron (II) is oxidized to iron (III) [2]. L-subunits lack the ferroxidase site and mainly provide support to maintain the ferric oxide biomineral in a soluble form [3].

The molar ratio Fe: ferritin is variable depending on the relative abundance of different subunits. For instance, the ferritin molecules from the liver and spleen, which are rich in L-subunits, have a relatively high average iron content (at least 1500 Fe atoms per molecule) although serum ferritin (also L-rich) shows, comparatively, a lower iron content (<600 atoms Fe per ferritin molecule). On the other hand, H-rich ferritins from the heart and brain have a relatively lower average iron content (<1000 Fe atoms per molecule) [4]. Although L-ferritin functions are traditionally associated with intracellular iron storage, additional functions related to iron delivery, based on a transferrin independent mechanism, have been recently discovered [5]. Among them, specific receptors for H and L-ferritins chains, namely TfR1 and SCARA5 respectively, were found overexpressed in different types of malignant tumors [[6], [7], [8], [9]].

One of the hallmarks of cancer is the subversion of normal iron metabolism in a way that favors a net intracellular iron accumulation. In other words, in many malignant tumors, the pathways of iron intake, efflux, storage and regulation are all perturbed, suggesting that the reprograming of iron metabolism is a central aspect of tumor survival [10]. To ensure it, it is well recognized that many cancer cells upregulate proteins that are involved in iron uptake (i.e. TfR1), whereas others exhibit a decreased expression of iron efflux proteins, such as ferroportin (Fpn), both leading to an increase of iron labile pool [[11], [12], [13], [14]]. Therefore, a great number of approaches were developed in attempt to exploit iron homeostasis for therapeutic intervention. These range from strategies to deprive cancer cells of iron, thus impairing cell development and growth [15,16], to alternative approaches aimed at increasing iron levels and selectively trigger cytotoxic levels of reactive oxygen species (ROS) as occurs in the ascorbate therapy [17] and in the administration of ferroptosis-inducers [18].

Moreover, a significant increase in serum ferritin levels has been associated to the presence of pathological processes, including inflammation, angiogenesis, and tumor formation. On this basis, it was surmised that serum ferritins (usually rich in L-chains) can act as potential biomarker of a given disease, useful for clinic diagnosis [19]. Tumor lysates from human breast cancer also show elevated levels of L-ferritin and this increase correlates with advanced histological grade and shorter survival times [20]. Moreover, in breast cancer cells the expression of iron importer genes is increased, whereas the expression of ferroportin is decreased to satisfy their increased demand for iron [21]. Although several studies have reported to show that serum ferritin is mainly secreted by hepatocytes, macrophages and Kupffer cells, the determinants of the increased serum ferritin, in the clinical context of oncology, still appears an unanswered issue [19].

In this context, taking advantage of the ferritin properties, such as its high stability, biocompatibility, ability to disassemble and reassemble in a shape memory fashion, different compounds with antineoplastic activity were successfully encapsulated into ferritin nanocages, such as cisplatin [22,23], doxorubicin [24], radioisotopes [25], curcumin [6,26], as well as, siRNA or miRNA [27]. These properties put ferritins ahead of conventional materials in clinical translation for drug delivery approaches in tumor treatment.

The toxic properties of Horse Spleen Ferritin (HoS-ferritin) and human H-Ferritin were recently reported by our group to explore a novel cancer therapy, tested in vitro on Hela cells, based on an iron dependent-mechanism that leads to cell death [28]. It was demonstrated that the toxicity of iron dependent-mechanisms may be the consequence of a mobile iron pool and of its lability at the low pH encountered during the endosomal import.

The aim of this study is to get more insight into the novel therapeutic strategy exploring the properties of the HoS-ferritin toxic potential in an in vitro and in vivo model of murine breast cancer. Moreover, the HoS-ferritin ability to generate contrast in a T2 weighted MR image was used to evaluate its biodistribution. The obtained results open new routes in the field of imaging guided tumor therapies based on an iron dependent mechanism of cancer cell damage.

2. **Methods**

2.1. Ferritin

Iron-loaded ferritin (HoS-ferritin-1000 Fe atoms) and apoferritin (HoS-apoferritin without Fe atoms) from equine spleen reported to contain 85% of L- and 15% of H-ferritin chains, were purchased from Sigma-Aldrich (St. Louis, MO). The number of Fe/cage in HoS-ferritin was measured by inductively coupled plasma mass spectrometry (ICP-MS). The protein concentration was determined by the Bradford assay.

2.2. Inductively coupled plasma mass spectrometry (ICP-MS)

Fe content into incubation media, cells and tissue samples were determined using ICP-MS (Element-2; Thermo-Finnigan, Rodano (MI), Italy) at medium mass resolution (M/ΔM ~ 4000) (see Supporting Information).

2.3. Cell lines

TS/A and NMuMG cells (kindly provided by prof. F. Cavallo's group, University of Turin), derived from a spontaneous BALB/c mammary carcinoma and from a benign cystadenoma of murine mammary gland, respectively, were used. TS/A were cultured in RPMI-1640 (Lonza) supplemented with 10% (v/v) fetal bovine serum (FBS), 2 mM l-glutamine, 100 U/ml penicillin and 100 U/ml streptomycin (Pen/Strep). NMuMG cells were cultured in DMEM medium supplemented with 10% (v/v) fetal bovine serum, 2 mM l-glutamine, 10 μg/ml insulin (Sigma), 100 U/ml penicillin and 100 U/ml streptomycin. Cells were incubated at 37 °C in a humidified atmosphere of 5% CO2. The cell lines were routinely tested to make sure of the absence of mycoplasma contamination (MycoAlert™ OLUS Mycoplasma Detection kit, Lonza). The iron content measured by ICP-MS in the two incubation cell media (inclusive of 10% FBS) resulted not significantly different (Fig. S1).

2.4. Internalization of HoS-ferritin by TS/A and NMuMG cells

HoS-ferritin uptake was assessed by the following methods: a) ICP-MS: TS/A and NMuMG cells were seeded at a density of 6 × 105 cells in a 25 cm2 culture flask and placed in a wet (37 °C) 5% CO2 air atmosphere incubator. At 24 h post seeding, cells were incubated with increasing concentrations of the above-mentioned HoS-ferritin. After 24 h of incubation, cells were washed three times with ice-cold phosphate-buffered saline (PBS), detached with trypsin/ethylenediaminetetraacetic acid (EDTA) and collected in 200 μl PBS. After sonication at 30% power for 30 s in ice, the protein content of cells was determined by Bradford assay and then cells were mineralized in 70% nitric acid. The Fe content in each cell line was determined by ICP-MS. The results were expressed as mol Fe/mg protein. b) For competition assay, TS/A were seeded at a density of 6 × 105 cells in a 25 cm2 culture flask and placed in a wet (37 °C) 5% CO2 air atmosphere incubator. At 24 h post seeding, cells were incubated for 6 h with 1 μM of HoS-ferritin in the presence or in the absence of 15 μM HoS-apoferritin pre-incubated 1.5 h before. At the end of the incubation, TS/A cells were washed with PBS, detached with trypsin-EDTA and collected in 200 μl of PBS. Then, they were sonicated and their protein content was measured by Bradford assay. Finally, they were mineralized and the

Fe content was measured by ICP-MS. c) Magnetic Resonance Imaging (MRI): glass capillaries containing 1 × 106 cells were placed in an agar phantom and MRI was performed using a T2-weighted RARE sequence protocol (TR/TE/NEX = 5000/53/4; FOV 1.2 cm; MTX 128 × 128). All the MR images were acquired on a Bruker Avance 300 spectrometer (7 T) with a Micro 2.5 microimaging probe (Bruker BioSpin). 1/T2 relaxation rates were determined using a MSME multislice multiecho sequence; d) Histological Perls' Prussian Blue method: 12.5 × 104 TS/A cells were seeded on glass bottom confocal dishes, incubated with HoS-ferritin for 24 h, washed with PBS, fixed 20 min at RT using PFA 4%, incubated with Prussian blue reactive according to Bunting [29] and examined under an optical microscope (Olympus BX14); e) Transmission electron microscopy (TEM): TS/A cells were seeded at a density of 1.5 × 106 in a T75 flask and treated with 6 μM HoS-ferritin for 1 h, 6 h and 24 h. Control cells were incubated in the same conditions without ferritin addition. After incubation cells were washed with PBS, detached with trypsin/EDTA and fixed in glutaraldehyde 2.5% in 10 mM phosphate buffer (pH 7.2) over night at 4 °C; then post-fixed in OsO4 1% in the same buffer and dehydrated in an ascending series of ethanol to 100%, incubated in two changes of absolute acetone, infiltrated in Epon-Araldite resin. The resin was polymerized for 24 h at 60 °C. Semi-thin sections of 1 μm were stained with 1% toluidine blue and ultra-thin (70 nm) sections were counter-stained with uranyl acetate and lead citrate and viewed with JEM-1010 transmission electron microscope (JEOL).

2.5. MTT assay

TS/A and NMuMG cells were seeded at a density of 8 × 103 cells/well in 96-well cell culture plates and then exposed to HoS-ferritin at a concentration range 1-6 μM for 24 h. At the end of the incubation, the cells were washed with PBS and cell vitality was evaluated using the MTT [3-(4,5-dimethylthiazol-2-yl)-2–5-dyphenyl single bond2H tetrazolium bromide] assay (Sigma-Aldrich) dissolved in medium at the concentration of 0.45 mg/ml. After 4 h, the supernatant was removed and the precipitated formazan was dissolved in 150 μl of DMSO and the microplate was incubated at room temperature for 30 min. Finally, absorbance was read at 570 nm with iMark microplate reader (Biorad). Cell vitality was reported as percentage of death cells observed in treated samples relative to that observed in control cells. The experiment was performed in triplicate and the data were graphically presented as mean ± SD.

2.6. Caspase-3/7 activity analysis

TS/A and NMuMG cells were seeded at a density of 3 × 105 cells in 3.5 cm diameter dishes and incubated for 3 h, 6 h and 24 h with 6 μM of HoS-ferritin. Cell caspase activity was assayed using the Muse Caspase 3/7 Assay Kit according to the user's guide. (see Supporting Information).

2.7. Evaluation of ROS production

Intracellular ROS production was detected using the Muse™ Oxidative Stress Kit (see Supporting Information).

2.8. TUNEL assay

TS/A cells were seeded at a density of 1.5 × 106 in a T75 flask, treated with 6 μM HoS-ferritin for 24 h, washed with PBS and detached with trypsin/EDTA. Cell suspensions containing 2 × 106 cells/ml were used to generate cytospin slides, which were fixed with PFA 4% at room temperature (RT) for 20 min and stained with the In situ Apoptosis Detection Kit (Abcam) according to manufacturer protocol.

2.9. Immunofluorescence studies

TS/A and NMuMG cells were seeded in a Ibidi μ-Slide 8 well at a density of 2 × 104 cells/well and incubated at 37 °C and 5% CO2 for 24 h in order to allow them to adhere to the slide surface. Then, cells were washed 3 times with PBS and fixed in cold methanol at 4 °C for 10 min. Then, cells where rinsed twice with PBS for 10 min. In order to block the non-specific binding sites, cells were treated with 5% normal goat serum for 30 min. Then, cells were incubated overnight at 4 °C with a rabbit polyclonal IgG1 anti-SCARA5 1:100 in PBS (sc-98,123 from Santa Cruz Biotechnology Inc., Dallas, Texas, USA), mouse monoclonal IgG1 anti-CD71 1:100 in PBS (sc-393,719 from Santa Cruz Biotechnology Inc., Dallas, Texas, USA) or mouse monoclonal IgG1 anti-LAMP-1 1:100 in PBS (sc-20,011 from Santa Cruz Biotechnology Inc., Dallas, Texas, USA). After the incubation, cells were washed twice in PBS for 10 min and they were incubated with a goat anti-mouse IgG (H + L) cross-adsorbed secondary antibody, Alexa Fluor 488 1:500 in PBS (A-11001, Invitrogen), goat anti-rabbit IgG (H + L) cross-adsorbed secondary antibody, Alexa Fluor 488 1:500 in PBS (A-11008, Invitrogen), or goat anti-mouse IgG (H + L) cross-adsorbed secondary antibody, Texas Red-X 1:500 in PBS (T-6390, Invitrogen) for 1 h at room temperature. Then, cells were washed 3 times for 10 min with PBS and air dried. Nuclei were counterstained with TO-PRO3 (T3605 Invitrogen). Coverslips were mounted with a glycerol/water solution (1/1, v/v). Observations were conducted under a confocal microscopy (Leica SP8 imaging system).

2.10. Orthotropic breast cancer model

All animal experiments were approved by the University Ethical Committee and performed in accordance with the European guidelines under directive 2010/63. Animals were purchased from Envigo Laboratories (Italy) and maintained in specific pathogen-free conditions. Breast tumors were generated in eight weeks old female BALB/c mice as follow: 3 × 105 TS/A cells were inoculated subcutaneously at the level of the left 5th mammary gland. Mice were examined twice a week until the tumor reached a volume of 40 mm3.

2.11. HoS-ferritin MR imaging

To evaluate the efficiency of HoS-ferritin as a natural contrast agent for MRI studies, three mice were treated with 90 mg/kg HoS-ferritin (11.2 mg/kg of iron i.v). Before MRI acquisition, animals were anesthetized by injecting tiletamine/zolazepam (Zoletil 100, Virbac, Milan, Italy) 20 mg/kg and xylazine (Rompun; Bayer, Milan, Italy) 5 mg/kg. MR images were acquired in each animal before the administration of the compound an after 3 h, 6 h and 24 h using a T2-weighted RARE sequence protocol (TR/TR/NEX = 5000/28/2; FOV = 2.8 cm; MTX 128 × 128) (see Supporting Information).

2.12. Schedule treatment of mice bearing tumor

Fig. S3 describes the schedule used to evaluate the in vivo efficiency of the HoS-ferritin against tumor growth. When tumors reached a volume of 40 mm3, mice were randomized in three groups (each one of n = 10). The first group was treated with 45 mg/kg HoS-ferritin (5.6 mg/kg of iron i.v.), the second with 45 mg/kg HoS-apoferritin and the third group received an equal volume of saline solution (vehicle) every three days for fifteen days. Tumor growth was monitored twice a week with MRI. At the end of the schedule mice were anesthetized and by mean of a medial laparotomy, a blood sample was taken from the posterior cava vein. Then the animals were euthanized. Fragments of liver, spleen, tumor, muscle, brain, kidneys and lungs were collected to determine the iron content by ICP-MS and for histological evaluations.

2.13. Histological studies

Tumors from the different groups were excised, hemi sectioned, photographed and then placed overnight in buffered 4% formaldehyde solution. Idem for fragments obtained from liver and spleen. Dewaxed 5 μm sections were stained with haematoxylin-eosin, Perls' Prussian blue, TUNEL and chloroacetate esterase staining.

2.14. AST activity evaluation

The potential toxicity of the HoS-ferritin to the liver was evaluated in terms of aspartate transaminase (AST) activity in plasma samples using AST activity assay kit (Sigma Aldrich). AST activity is reported as milliunit/ml.

2.15. Determination of [Fe] concentration in tissues by MRI

From the analysis of signal intensity change before and after HoS-ferritin administration (Eq. 1) it was possible to calculate the [Fe] concentration in tumor and liver and compare it with the corresponding values obtained by ICP-MS.

$$\frac{SI(PRE)}{SI(POST)} = \frac{((1-\exp((-TR-TE)R1(PRE)))*\exp(-TE*R2))}{((1-\exp((-TR-TE)R1(POST)))*\exp(-TE*R2))}$$

The R2 precontrast (R2(PRE)) maps were obtained by using a Spin-Echo sequence; R2 post-contrast (R2(POST)) maps were calculated by using the PRE- and POST-contrast SI ratio [Eq. (1)] measured in the regions of interest, which were manually drawn on T2-weighted images; r2p is the millimolar relaxivity of HoS-ferritin at 7 T (2.9 mM−1 s−1). In Eq. (1) [29]. TR represents the repetition time, TE is the echo time, and R1 and R2 are the water proton relaxation times.

3. **Results**

3.1. Cell uptake of HoS-ferritin

In order to assess the expression of TfR1[30,31] and SCARA5 receptors involved in the recognition and uptake of the H– and L- ferritin chains, respectively, fluorescence microscopy

studies were performed on TS/A and NMuMG cell lines. Although both receptors were present in both cell lines, SCARA5 appeared to be more expressed in TS/A cells with respect to NMuMG (Supplementary Information, Fig. S4), while no difference in TfR1 receptor was assessed between the two cell lines.

Then, the ability of TS/A cells to take up ferritin from the incubation media, compared to the more differentiated NMuMG cells isolated from a benign cystadenoma of the mammary gland was assessed. For this purpose, HoS-ferritin, containing ca. 1000 iron atoms per protein, was used without any further modification. The experimental protocol was based on the measurement of the amount of iron internalized by these two cell lines, upon 24 h incubation in the presence of HoS-ferritin, at 37 °C and 5% CO2. Cell iron content was determined by Inductively Coupled Plasma Mass Spectroscopy (ICP-MS). As reported in Fig. 1A the amount of Fe internalized by TS/A cells was >2-fold the values found for NMuMG cells ($p = .0023$).

In order to assess whether ferritin can be exploited as a MRI probe for tumor detection, T2-weighted MR images were acquired on TS/A and NMuMG cellular pellets upon 24 h incubation in the presence of 3 μM of HoS-ferritin. Cells were washed, detached from the flasks with trypsin/EDTA, transferred into glass capillaries and placed in an agar phantom to acquire MR images at 7 T. As control, the cells were incubated in the same medium without HoS-ferritin. Fig. 1B shows that TS/A cells incubated with HoS-ferritin displayed a marked decrease in the signal intensity (SI) when compared to untreated cells, while only small changes in SI were observed in the case of NMuMG cells either incubated with or without HoS-ferritin. The low SI is the result of the superparamagnetic ferrihydrite crystal ($5Fe_2O_3 \times 9H_2O$) contained in the inner protein cavity that accelerates the transverse NMR relaxation rate ($R2 = 1/T2$) of solvent water protons, causing a negative contrast in the corresponding MR image [32]. The differences among the relaxation rates R2 (s^{-1}) measured on the same cell pellets reflected the observed difference in HoS-ferritin uptake by TS/A and NMuMG as expected by their different ferritin receptors expression (Fig. 1C).

As NMuMG cells exhibit a lower expression of SCARA5 (Supplementary Information, Fig. S4) their capacity to incorporate Fe not bound to transferrin appears to be minimal. Moreover, in order to exclude an aspecific internalization of Fe, a competition assay was performed pre-incubating TS/A cells (1.5 h) with an excess of HoS-apoferritin (15:1) before adding HoS-ferritin (1 μM) for 6 h. After the incubation of HoS-ferritin in the presence of HoS-apoferritin, a reduction of internalized Fe (about 40%, Fig. S2) was observed with respect to TS/A treated only with HoS-ferritin. This result demonstrates that the internalization of iron is driven by receptor mediated endocytosis through HoS-apoferritin receptors [6,26]. Finally, to get more insight into the intracellular iron localization, the iron incorporated by TS/A cells was also detected by the Perls' Prussian blue histochemical method and by TEM. After 24 h of incubation, most of the TS/A cells showed granular Prussian blue deposits (Supplementary Information, Fig. S5). Clusters of electron dense iron cores were also observed by TEM at level of the endolysosomal compartment (ELC) (Fig. 2). It is interesting to point up that electron

dense area were also observed in zones of plasma membrane invagination, as well as in small endocytic vesicles (SEV) (Fig. 2A). TEM images reveal that these SEV enter in the endocytic degradative pathway by fusing with early endosomes (Fig. 2B), then transported to late endosome via the organization of multivesicular bodies (MVB) to form occasionally hybrid organelles with late lysosomes. In these vesicles, at least in part, ferritin was degraded to form electron- dense particles of variable size, ranging from few nanometers to long specular crystals i.e. hemosiderin (Fig. 2C-D) [33,34]. Confocal microscopy showed that TS/A cells treated with HoS-ferritin show an expansion of the endolysosomal compartment (ELC) respect to the non-treated cells. Furthermore, HoS-ferritin treated cells exhibited a large lysosome clustering (Supplementary Information, Fig. S6). From these observations one can draw the conclusion that, after the binding to its receptor, HoS-ferritin undergoes the endocytic degradative pathway.

3.2. HoS-ferritin toxicity

To evaluate the toxic action of the HoS-ferritin toward TS/A and NMuMG cells, cell vitality was determined by the MTT assay after 24 h of incubation with different concentration of HoS-ferritin (1–6 μM). The toxicity of HoS-ferritin against TS/A cells was higher with respect to NMuMG (Fig. 3A). In fact, in the presence of 3 μM and 6 μM HoS-ferritin, cell vitality was significantly reduced to 42 ± 4 and 5.0 ± 0.6% for TS/A, and 85 ± 2 and 18 ± 1% for NMuMG, respectively, compared with untreated cells. According to MTT results, TS/A cells display a better correlation between mol Fe/mg protein and cell vitality (Pearson's r = −0.93, **P = .003) compared to NMuMG cells (Pearson's r = −0.74, *P = .01) (Fig. 3B and C).

Cytoplasmic ROS production was evaluated in TS/A cells incubated for 24 h with HoS-ferritin. Fig. 4A shows that cells positive to ROS cytofluorimetric test were 47 ± 1 and 69 ± 6% for cells incubated with HoS-ferritin 3 μM and 6 μM, respectively, with respect to a 20% of untreated cells.

The activation of caspase 3/7 after treatment with 3 μM and 6 μM of HoS-ferritin has been also evaluated. To note, the percentage of cells defined as “late apoptosis” and those defined as “cell dead” (see material and methods for details) increased significantly with the incubation time, particularly when cells were treated with 6 μM of HoS-ferritin (Fig. 4B). The assessment of ROS production and caspase 3/7 activity were also performed on NMuMG in addition to TS/A cells (Fig. 4 C and D). Panel C shows that, upon the incubation in the presence of 3 or 6 μM HoS-ferritin, the ROS+ cells still remain at the baseline level as in untreated control cells. Moreover, panel D (caspase 3/7 assay) shows that, increasing the incubation time in the presence of HoS-ferritin (6 μM) in NMuMG cells, the apoptotic profile does not change significantly evidencing >60% of live cells in all the considered conditions.

Moreover, consistently with ROS production, we observed increased frequency of TUNEL-positive cells in TS/A cells treated with 6 μM HoS-ferritin for 24 h (Supplementary Information, Fig. S7). Examination of TEM images confirms this hypothesis, showing cells with the typical

features of apoptosis, i.e. shrunken cytoplasm, dense, deeply stained chromatin and the presence of budding and blebbing processes (Supplementary Information, Fig. S8A). Concerning oncosis, most probably cells begin to die by apoptosis, but if ATP depletion occurs during downstream apoptotic signaling a suddenly cut off of the sequence of apoptosis may take place and then necrapoptosis may occur [35]. Features of cells in necrapoptosis are practically indistinguishable from those undergoing classical oncosis. Clumps of chromatin with ill-defined edges, swollen cytoplasm and organelles and loss of plasma membrane integrity are observed in both cases (Supplementary Information, Fig. S8B).

TS/A cells incubated for 24 h in the presence of 6 μM HoS-ferritin showed numerous auto-phagosomes sequestering hemosiderin and incipient lamellar bodies (Supplementary Information, Fig. S9). One may surmise that these observations report on a defense mechanism activated by cells to avoid the point of non-return. Accordingly with our observation, in a recent publication Krenn et al. [36] reported that ferritin-mediated lysosomal stress stimulates macroautophagy in an attempt to transfer antioxidants, including cytosolic apoferritin, to iron–overloaded lysosomes, in order to avoid Fenton mediated oxidative stress [36].

3.3. Tumor MRI visualization of HoS-ferritin uptake

The efficacy of HoS-ferritin as a kind of “natural theranostic agent” was assessed in vivo on a mice model of orthotopic breast cancer, generated by subcutaneous injection of TS/A cells in BALB/c mice. When the tumors reached a volume of approximately 40 mm3, mice were treated with HoS-ferritin (90 mg/kg of protein, i.v.). The T2-weigted MR image confirmed that the dose of HoS-ferritin administered was enough to induce a well detectable negative contrast. From the analysis of the signal intensity (SI) a small but significant decrease in the tumor region (−6.6%) was detected 3 h after HoS-Ferritin injection, while the maximum negative contrast (−8.7%) was observed in the tumor after 6 h (Fig. 5C). After 24 h the signal attributable to the administered HoS-ferritin was still detectable in the tumor (−5.9%). After HoS-ferritin administration, the maximum SI decrease was observed in the liver (−40%) and did not change up to 24 h.

Animals were sacrificed 24 h after the intravenous injection of HoS-ferritin. ICP-MS analysis of iron content was performed ex vivo in liver, spleen, tumor and muscle. A significant increase in iron content was observed in the liver ($p = .007$) and tumor ($p = .01$) with respect to vehicle treated mice (Fig. 5B).

From the analysis of signal intensity change before and after HoS-ferritin administration (see methods, Eq. 1) it was possible to calculate the [Fe] concentration in tumor and liver and compare it with the corresponding values obtained by ICP-MS. (Table 1).

3.4. Tumor treatment

To investigate the toxic properties of HoS-ferritin assessed in the in vitro studies on TS/A cells, an in vivo study using the murine model of TS/A breast cancer was assessed as a non-conventional therapeutic strategy by the treatment with HoS-ferritin.

According with the schedule showed in Fig. S3, tumor volume was measured by MRI, the day after each HoS-ferritin administration (45 mg/kg /i.v). After the 4th dose we observed a significant reduction of the tumor volume (1.6-fold decrease, $p < .05$) in comparison to mice treated with the vehicle alone (0.9% NaCl) and with the same amount of HoS-apoferritin (Fig. 6).

After the 5th dose, the tumors treated with HoS-ferritin showed a brighter inhomogeneous area in the T2-weighted MR image, in contrast with the homogeneous signal showed in the vehicle treated mice. The ex vivo macroscopic examination of the neoplasms showed extensive soft gray-white areas that were confirmed by the histological observation. Sections stained with H&E showed extensive areas of coagulative necrosis in contrast with the small and isolated foci of coagulative necrosis present in the tumors treated with the vehicle and HoS-apoferritin (Fig. 7).

As it was observed in the in vitro treatment, numerous TUNEL positive tumors cells were detected in the interface between the non-necrotic tumor and the coagulative necrotic zones (Supplementary Information, Fig. S10). Since the number of inflammatory cells present in the TS/A neoplasms were scanty (Supplementary Information, Fig. S11), one may surmise that the extensive areas of necrosis, generated after the fifth cycle of HoS-ferritin treatment, can be considered secondary necrosis. In fact, a huge release of apoptotic bodies, which overwhelms the clearance capacity of phagocytes, can progress to loss of membrane integrity and autolysis [37]. Most probably, the release of damage associated molecular patterns by the secondary necrotic cells were able to attract pro-inflammatory innate immune cells from the blood, i.e. neutrophils, organizing an inflammatory reaction, practically absent in mice treated with physiological solution (Supplementary Information, Fig. S12 and Table S1).

At the end of the treatment, mice were sacrificed and tissue specimens from tumor, liver, spleen, muscle, brain, kidney and lungs were obtained to measure the iron content by ICP-MS. Fig. 8J shows that iron concentration is two and three times higher in the tumor and liver of HoS-ferritin treated mice, than in HoS-apoferritin and vehicle control mice, respectively. Instead, iron levels were maintained stable in the spleen, muscle, brain, kidneys and lungs for all experimental groups (Supplementary Information, Fig. S13). This is an indication that ferritin receptors present in tissue organs (brain, lungs, kidneys) besides tumor and liver appear not sufficiently up-regulated to pursue large internalization of the protein. Moreover, we cannot assess whether a low extravasation of this high molecular weight protein (450 KDa) may prevent to access to the extracellular space. Prussian blue stain, which detects iron accumulated by cells, showed positive cells in HoS-ferritin treated tumors, as well as in the liver, particularly at level of Kupffer cells, suggesting an active capacity to sequester exogenous ferritin by these cells (Fig. 8A-I). The potential toxicity of HoS-ferritin, in particular toward the liver, was evaluated in terms of AST activity in plasma samples. No significant

differences were found between the treated and the control groups. These results indicate the absence of liver damage owing to iron accumulation, also confirmed by histological analysis (Supplementary Information, Fig. S14).

4. **Discussion**

Main efforts in cancer therapy are devoted on the development of highly accurate and specific tools for early detection of cancer onset, and its personalized therapy. In this context, ferritin holds a tremendous potential as a device for theranostic applications. By exploiting the natural recognition of its specific receptors (TfR1 and SCARA5 for H– and L-chains, respectively), ferritin nanocages may ensure a proper drug delivery and release with notably specificity [[6], [7], [8], [9]]. Although, TfR1 was already successfully exploited for targeted therapy using antibodies in preclinical models [37], SCARA5 expression has not been comprehensively examined in tumor tissues. Herein we demonstrated that SCARA5 can be used as specific receptor to deliver toxic iron payload to breast tumor cells. We think that the exploitation of the natural receptors for ferritin could be an advantage for the simplicity of the preparation protocol that may became easily translated to the clinical use. In alternative, HoS-ferritin or ferritin of human origin may be functionalized with specific ligands (i.e. folate, peptides, aminoacids) that have receptors overexpressed at the tumor site [38,39].

Due to its ability to gain and lose electrons, iron is able to participate in potentially harmful reactions, such as the Fenton mediated generation of ROS, in which the ferrous iron reacts with hydrogen peroxide to yield hydroxyl radical. This reaction not only damage lipids and proteins, but also cause oxidative damage of DNA [40]. As endocytosed ferritin is translocated to the ELC, its iron content is released by proteolytic degradation [41]. Based on these observations, it can be surmised that endocytosis of extracellular ferritin increases the level of free ferrous iron in the ELC, promoting Fenton chemistry-based oxidative stress and lysosomal membrane disruption. Subsequently, the release of reactive lysosomal content leads to cellular damage, activation of executive caspases and the activation of the death pathway by apoptosis and oncosis (necrapoptosis) [42,43]. Moreover, endocytosed HoS-ferritin (isoelectric point = 4.4) [44] can act as a proton sponge that could be responsible of an osmotic pressure increase across the lysosomal membrane which causes the inflow of water leading to disruption of the vesicle [45].

In the past we and others have pursued the loading of ferritin with paramagnetic species such as Gd-HPDO3A, MnOOOH, iron oxide particles [[46], [47], [48]] in order to yield efficient contrast agents for MRI [49]. Herein it has been shown that the administration of HoS-ferritin can be used, without any modification, to visualize tumor cells by MRI (see Fig. 1, Fig. 5, Fig. 7).

Moreover, though the ferritin used in this study was isolated from equine spleen, we can reasonably exclude immunogenicity problems due to the high sequence homology of the horse and mouse ferritin, with most amino acid changes resulting in amino acids with the same charge and only very minor changes to the structure [50]. The herein reported results demonstrate a lack of significant detrimental effects of HoS-ferritin at MRI-detectable doses, allowing further exploration of this theranostic agent in basic oncology research. Moreover, these results may prompt new insights in the exploitation of the interesting achievements

obtained when the expression of ferritin is used as a imaging gene reporter [51]. It would be interesting to assess whether the different localization site of ferritin (cytoplasm vs. endosomes) may trigger differences in its toxic effects to tumor cells. The idea that iron overload can selectively inhibit tumor growth is largely unexplored. There are only few examples in the literature regarding this topic [28,52,53]. One of them was reported by Kiessling et al., in 2009, that demonstrated as a proof of concept the toxic effect of iron in an aggressive T-cell lymphoma [52]. In fact, they found that, by blocking the production of the iron storage protein ferritin H-chain, there is an increase in the intracellular labile iron pool that results in an increase of ROS generation and, in turn, in significant effects on tumor growth, while normal cells were unharmed.

The results herein described show for the first time in vivo on a preclinical model, that iron overdose delivered by the ferritin nanocage of natural origin can trigger selective mechanisms of regulated cell death in cancer cells.

Declaration of Competing Interest

The authors declare that there is no conflict of interest regarding the publication of this article.

Acknowledgments

We aknowledge Regione Piemonte for funding to the Green Factory For Composites, the Italian Ministry for Education and Research (MIUR) for yearly FOE funding to the Euro-BioImaging Multi-Modal Molecular Imaging Italian Node (MMMI) and for PRIN code 2012SK7ASN.

References

[1] Z. Zhen, W. Tang, T. Todd, J. Xie, Ferritins as nanoplatforms for imaging and drug delivery, Expert Opin. Drug Deliv. 11 (12) (2014) 1913–1922.

[2] C. Pozzi, F. Di Pisa, C. Bernacchioni, S. Ciambellotti, P. Turano, S. Mangani, Iron binding to human heavy-chain ferritin, Acta Crystallogr. Sect. D Biol. Crystallogr. 71 (2015) 1909–1920.

[3] P. Santambrogio, S. Levi, A. Cozzi, B. Corsi, P. Arosio, Evidence that the specificity of iron incorporation into homopolymers of human ferritin L- and H-chains is conferred by the nucleation and ferroxidase centres, Biochem. J. 314 (1996)

139–144.

[4] J. Alonso García, D. Turiel Fernández, E. Añón Álvarez, E. Blanco González,

M. Montes-Bayón, A. Sanz-Medel, Iron speciation, ferritin concentrations and Fe:ferritin ratios in different malignant breast cancer cell lines: on the search for cancer biomarkers, Metallomics. 8 (10) (2016) 1090–1096.

[5] J. Fisher, K. Devraj, J. Ingram, et al., Ferritin: a novel mechanism for delivery of iron to the brain and other organs, Am. J. Physiol. Physiol. 293 (2) (2007) C641–C649.

[6] L. Conti, S. Lanzardo, R. Ruiu, et al., L-ferritin targets breast cancer stem cells and delivers therapeutic and imaging agents, Oncotarget. 7 (41) (2016) 66713–66727.

[7] L.N. Turino, M.R. Ruggiero, R. Stefanìa, J.C. Cutrin, S. Aime, S. Geninatti Crich, Ferritin decorated PLGA/paclitaxel loaded nanoparticles endowed with an en- hanced toxicity toward MCF-7 breast tumor cells, Bioconjug. Chem. 28 (4) (2017) 1283–1290.

[8] B. Du, S. Jia, Q. Wang, et al., A self-targeting, dual ROS/pH-responsive Apoferritin nanocage for spatiotemporally controlled drug delivery to breast cancer, Biomacromolecules 19 (3) (2018) 1026–1036.

[9] Y. Liu, Y.R. Tan, W.W. Sun, et al., Identification of SCARA5 as a potential biomarker for oral squamous cell Carcinoma using MALDI–TOF–MS analysis, Proteomics Clin. Appl. 12 (5) (2018) 1–8.

[10] S.V. Torti, D.H. Manz, B.T. Pail, N. Blanchette-Farra, F.M. Torti, Iron and cancer, Annu. Rev. Nutr. 38 (2018) 97–125.

[11] T.R. Daniels, E. Bernabeu, J.A. Rodríguez, et al., The transferrin receptor and the targeted delivery of therapeutic agents against cancer, Biochim. Biophys. Acta Gen. Subj. 1820 (3) (2012) 291–317.

[12] R.S. Ohgami, D.R. Campagna, E.L. Greer, et al., Identification of a ferrireductase required for efficient transferrin-dependent iron uptake in erythroid cells, Nat. Genet. 37 (11) (2005) 1264–1269.

[13] E. Nemeth, M.S. Tuttle, J. Powelson, T. Ganz, J. Kaplan, Hepcidin regulates cellular Iron efflux by binding to Ferroportin and inducing its internalization, Science 306

(80) (2004) 2090–2094.

[14] Z.K. Pinnix, L.D. Miller, W. Wang, et al., Ferroportin and iron regulation in breast cancer progression and prognosis, Sci. Transl. Med. 2 (43) (2010) 43ra56-43ra56.

[15] T. Yamasaki, S. Terai, I. Sakaida, Deferoxamine for advanced hepatocellular car- cinoma, N. Engl. J. Med. 365 (6) (2011) 576–578.

[16] N. Gattermann, C. Finelli, M. Della Porta, et al., Deferasirox in iron-overloaded

patients with transfusion-dependent myelodysplastic syndromes: results from the large 1-year EPIC study, Leuk. Res. 34 (9) (2010) 1143–1150.

[17] J.D. Schoenfeld, Z.A. Sibenaller, K.A. Mapuskar, et al., O2·− and H2O2-mediated disruption of Fe metabolism causes the differential susceptibility of NSCLC and GBM cancer cells to pharmacological ascorbate, Cancer Cell 31 (2017) 487–500.

[18] W.S. Yang, B.R. Stockwell, Synthetic lethal screening identifies compounds acti- vating Iron-dependent, nonapoptotic cell death in oncogenic-RAS-harboring cancer cells, Chem. Biol. 15 (3) (2008) 234–245.

[19] K. Fan, L. Gao, X. Yan, Human ferritin for tumor detection and therapy, Wiley Interdiscip. Rev. Nanomed. Nanobiotechnol. 5 (4) (2013) 287–298.

[20] S.V. Chekhun, N.Y. Lukyanova, Y.V. Shvets, A.P. Burlaka, L.G. Buchynska, Significance of ferritin expression in formation of malignant phenotype of human breast cancer cells, Exp. Oncol. 36 (3) (2014) 179–183.

[21] X.P. Jiang, R.L. Elliott, J.F. Head, Manipulation of iron transporter genes results in the suppression of human and mouse mammary adenocarcinomas, Anticancer Res. 30 (3) (2010) 759–765.

[22] Z. Yang, X. Wang, H. Diao, et al., Encapsulation of platinum anticancer drugs by apoferritin, Chem. Commun. 7345 (33) (2007) 3453–3455.

[23] D.M. Monti, G. Ferraro, A. Merlino, Ferritin-based anticancer metallodrug delivery: crystallographic, analytical and cytotoxicity studies, Nanomed. Nanotechnol. Biol. Med. 20 (2019) 101997.

[24] Z. Zhen, W. Tang, H. Chen, et al., RGD-modified apoferritin nanoparticles for ef-

ficient drug delivery to tumors, ACS Nano 7 (6) (2013) 4830–4837.

[25] J.F. Hainfeld, Uranium-loaded apoferritin with antibodies attached: molecular de- sign for uranium neutron-capture therapy, Proc. Natl. Acad. Sci. 89 (22) (2006) 11064–11068.

[26] S. Geninatti Crich, M. Cadenazzi, S. Lanzardo, et al., Targeting ferritin receptors for the selective delivery of imaging and therapeutic agents to breast cancer cells, Nanoscale. 7 (15) (2015) 6527–6533.

[27] E.J. Lee, S.J. Lee, Y.S. Kang, et al., Engineered proteinticles for targeted delivery of siRNA to cancer cells, Adv. Funct. Mater. 25 (8) (2015) 1279–1286.

[28] J.C. Cutrin, D. Alberti, C. Bernacchioni, et al., Cancer cell death induced by ferritins and the peculiar role of their labile iron pool, Oncotarget. 9 (46) (2018)

27974–27984.

[29] L. Shiftan, T. Israely, M. Cohen, et al., Magnetic resonance imaging visualization of hyaluronidase in ovarian carcinoma, Cancer Res. 21 (2005) 10316–10324.

[30] H.O. Habashy, D.G. Powe, C.M. Staka, et al., Transferrin receptor (CD71) is a marker of poor prognosis in breast cancer and can predict response to tamoxifen, Breast Cancer Res. Treat. 119 (2) (2010) 283–293.

[31] D. Högemann-Savellano, E. Bos, C. Blondet, et al., The transferrin receptor: a po- tential molecular imaging marker for human cancer, Neoplasia. 5 (6) (2003) 495–506.

[32] Y. Gossuin, C. Burtea, A. Monseux, et al., Ferritin-induced relaxation in tissues: an in vitro study, J. Magn. Reson. Imaging 20 (4) (2004) 690–696.

[33] U. Repnik, M.H. Cesen, B. Turk, The endolysosomal system in cell death and sur- vival, Cold Spring Harb. Perspect. Biol. 5 (2013) 1–14.

[34] T.C. Iancu, Ultrastructural aspects of iron storage, transport and metabolism, J. Neural Transm. 118 (3) (2011) 329–335.

[35] H. Jaeschke, J.J. Lemasters, Apoptosis versus oncotic necrosis in hepatic ischemia/ reperfusion injury, Gastroenterology. 125 (4) (2003) 1246–1257.

[36] M.A. Krenn, M. Schürz, B. Teufl, K. Uchida, P.M. Eckl, N. Bresgen, Ferritin-stimu- lated lipid peroxidation, lysosomal leak, and macroautophagy promote lysosomal “metastability” in primary hepatocytes determining in vitro cell survival, Free Radic. Biol. Med. 80 (2015) 48–58.

[37] I.S. Trowbridge, F. Lopez, Monoclonal antibody to transferrin receptor blocks transferrin binding and inhibits human tumor cell growth in vitro, Proc. Natl. Acad. Sci. 79 (4) (1982) 1175–1179.

[38] V.V. Shuvaev, M. Khoshnejad, K.W. Pulsipher, et al., Biomaterials spatially con- trolled assembly of affinity ligand and enzyme cargo enables targeting ferritin na- nocarriers to caveolae, Biomaterials 185 (June) (2018) 348–359.

[39] M. Khoshnejad, H. Parhiz, V.V. Shuvaev, I.J. Dmochowski, V.R. Muzykantov, Ferritin-based drug delivery systems : hybrid nanocarriers for vascular im- munotargeting, J. Control. Release 282 (January) (2018) 13–24.

[40] S.V. Torti, F.M. Torti, Iron and cancer: more ore to be mined, Nat. Rev. Cancer 13

(5) (2013) 342–355.

[41] T.Z. Kidane, E. Sauble, M.C. Linder, Release of iron from ferritin requires lysosomal activity, Am. J. Physiol. Physiol. 291 (3) (2006) C445–C455.

[42] N. Bresgen, H. Jaksch, H. Lacher, I. Ohlenschläger, K. Uchida, P.M. Eckl, Iron- mediated oxidative stress plays an essential role in ferritin-induced cell death, Free Radic. Biol. Med. 48 (10) (2010) 1347–1357.

[43] M.E. Guicciardi, M. Leist, G.J. Gores, Lysosomes in cell death, Oncogene 23 (16 REV. ISS. 2) (2004) 2881–2890.

[44] A. Mazur, I. Litt, E. Shorr, Chemical properties of ferritin and their relation to its vasodepressor activity, J. Biol. Chem. 187 (1950) 473–484.

[45] T. Kurz, A. Terman, B. Gustafsson, U.T. Brunk, Lysosomes in iron metabolism, ageing and apoptosis, Histochem. Cell Biol. 129 (4) (2008) 389–406.

[46] S. Aime, L. Frullano, S. Geninatti Crich, Compartmentalization of a gadolinium complex in the Apoferritin cavity: a route to obtain high Relaxivity contrast agents for magnetic resonance imaging, Angew. Chem. Int. Ed. 41 (6) (2002) 1017–1019.

[47] F.K. Kálmán, S. Geninatti-Crich, S. Aime, Reduction/dissolution of a β-MnOOH nanophase in the ferritin cavity to yield a highly sensitive, biologically compatible magnetic resonance imaging agent, Angew. Chem. Int. Ed. 49 (3) (2010) 612–615.

[48] M. Ruggiero, D. Alberti, V. Bitonto, S. Geninatti Crich, Ferritin: a platform for MRI contrast agents delivery, Inorganics. 7 (3) (2019) 33.

[49] S. Geninatti Crich, B. Bussolati, L. Tei, et al., Magnetic resonance visualization of tumor angiogenesis by targeting neural cell adhesion molecules with the highly sensitive gadolinium-loaded apoferritin probe, Cancer Res. 66 (18) (2006) 9196–9201.

[50] S. Dostalova, H. Polanska, M. Svobodova, et al., Prostate-specific membrane an- tigen-targeted site-directed antibody-conjugated Apoferritin Nanovehicle favorably influences in vivo side effects of doxorubicin, Sci. Rep. 8 (1) (2018) 1–13.

[51] B. Cohen, H. Dafni, G. Meir, A. Harmelin, M. Neeman, Ferritin as an endogenous MRI reporter for noninvasive imaging of gene expression in C6 glioma tumors, Neoplasia. 7 (2) (2006) 109–117.

[52] M.K. Kiessling, C.D. Klemke, M.M. Kamiriski, I.E. Galani, P.H. Krammer, K. Giilow, Inhibition of constitutively activated nuclear factor-K,B induces reactive oxygen species- and iron-dependent cell death in cutaneous T-cell lymphoma, Cancer Res. 69 (6) (2009) 2365–2374.

[53] M. Poljak-Blazi, D. Stancic-Rokotov, A. Ferle-Vidovic, Inhibitory effect of iron on melanoma B16 growth, Period. Biol. 87 (1985) 17–21.

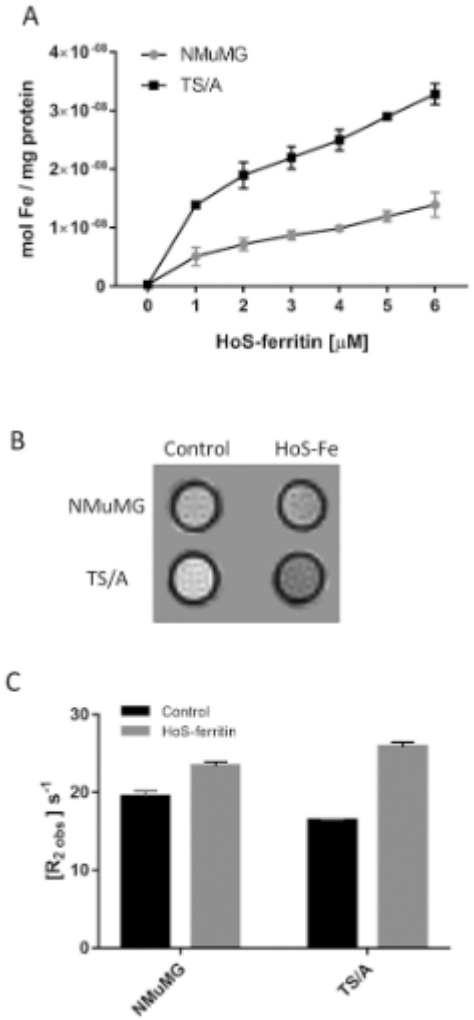

Fig. 1. Cellular uptake of HoS-ferritin by NMuMG and TS/A cell lines. (A) Cells were incubated 24 h at 37 °C in the presence of increasing concentrations of HoS-ferritin (1–6 μM). Iron internalization was measured by ICP-MS. The results are expressed as mean ± SD of 5 independent experiments. (B) A representative T_2-weighted RARE MR image of an agar phantom containing NMuMG and TS/A cells incubated or not for 24 h with HoS-ferritin 3 μM. (C) R_2 (s^{-1}) measured on cell pellets. The histogram shows the mean ± SD of 3 independent experiments.

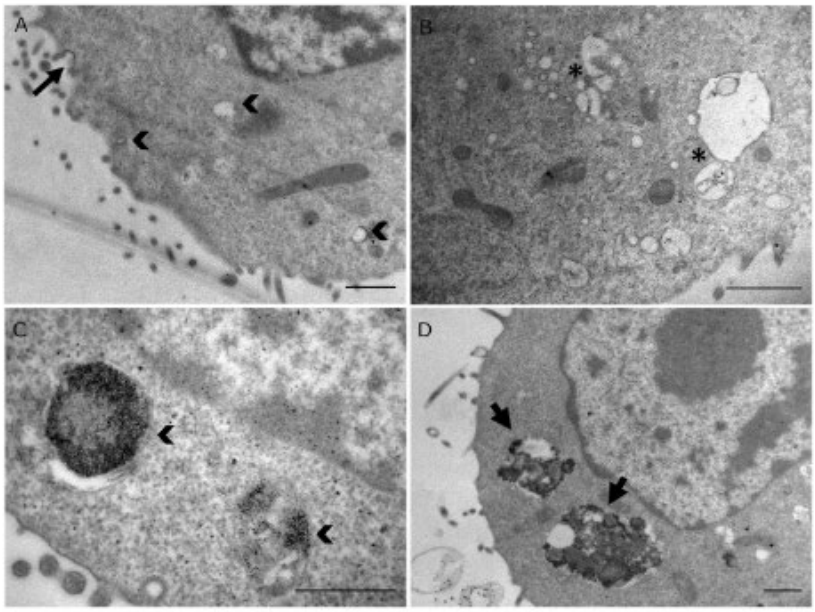

Fig. 2. TEM images of TS/A cells treated with 6 μM of HoS-ferritin for 1 h (A), 6 h (B) and 24 h (C, D). (A) Arrow indicates plasma membrane invagination; arrowheads indicate small endocytic vesicles (SEV) (magnification x20.000), scale bar − 0.2 μm. (B) Asterisks sign endocytic vesicles fusing with endosomes (magnification x30.000), scale bar − 0.2 μm. (C) Arrowheads indicate late endosomes containing hemosiderin particles (magnification x75.000), scale bar − 0.1 μm. (D) Arrows indicate multivesicular bodies (MVB) containing hemosiderin particles (magnification x15.000), scale bar − 0.2 μm.

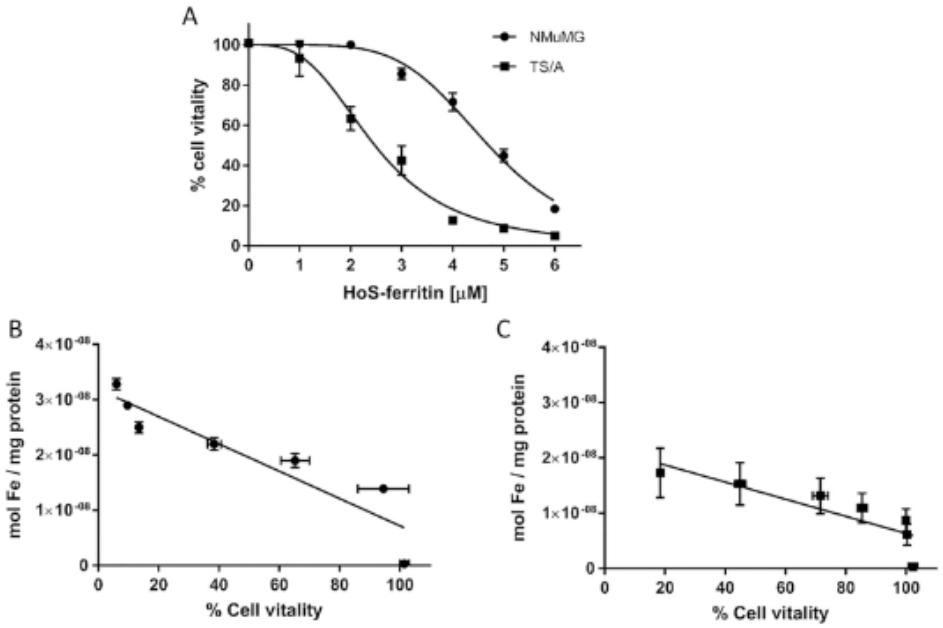

Fig. 3. (A) Percentage of vitality (measured by MTT assay) of TS/A and NMuMG after 24 h of incubation with different concentrations of HoS-ferritin. Graphs show the mean ± SD of percentage vitality evaluated on 3 independent experiments. Correlation between mol Fe/mg protein and cell vitality measured in TS/A (Pearson's r − −0.93, **P − .003) (B) and NMuMG (Pearson's r − −0.74, *P − .01) (C) after HoS-ferritin incubation.

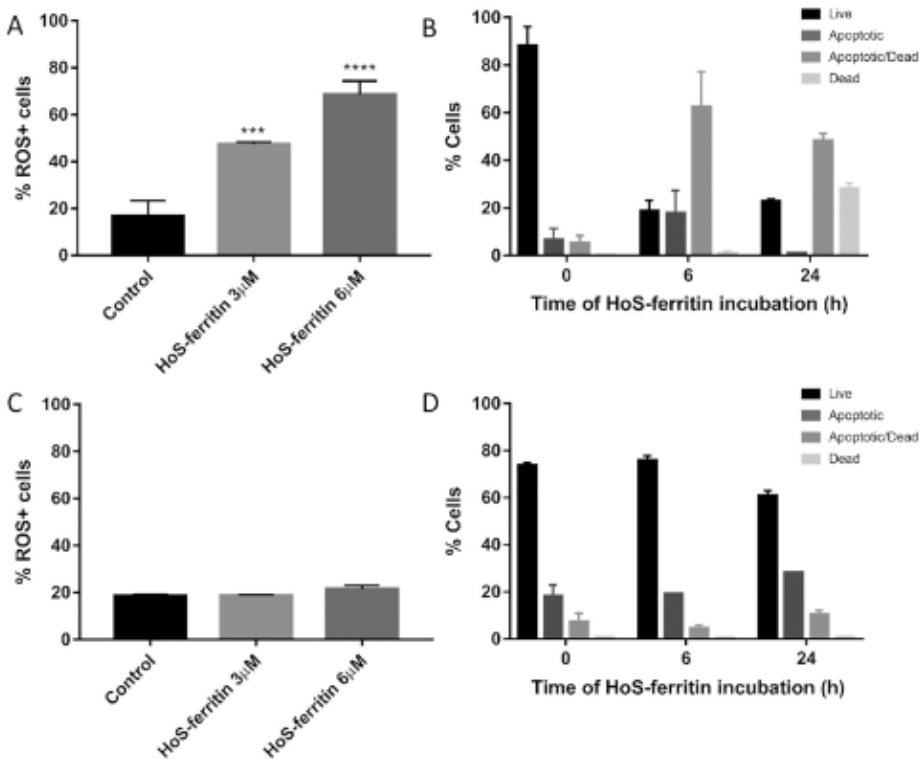

Fig. 4. Percentage of ROS positive TS/A (A) and NMuMG (C) cells in basal conditions and after 24 h of incubation with different concentrations of HoS-ferritin. Graphs show the mean ± SD of percentage of ROS positive cells evaluated on 3 independent experiments. Statistical analysis Turkey's multiple comparison test, ***$p < .001$, ****$p < .0001$. Analysis of caspase 3/7 activity using a flow cytometric assay in TS/A (B) and NMuMG (D) cells in basal conditions (time 0) and after treatment for 6 h and 24 h with 6 μM HoS-ferritin. The graphs represent percentage of live, apoptotic, apoptotic/dead and dead cells.

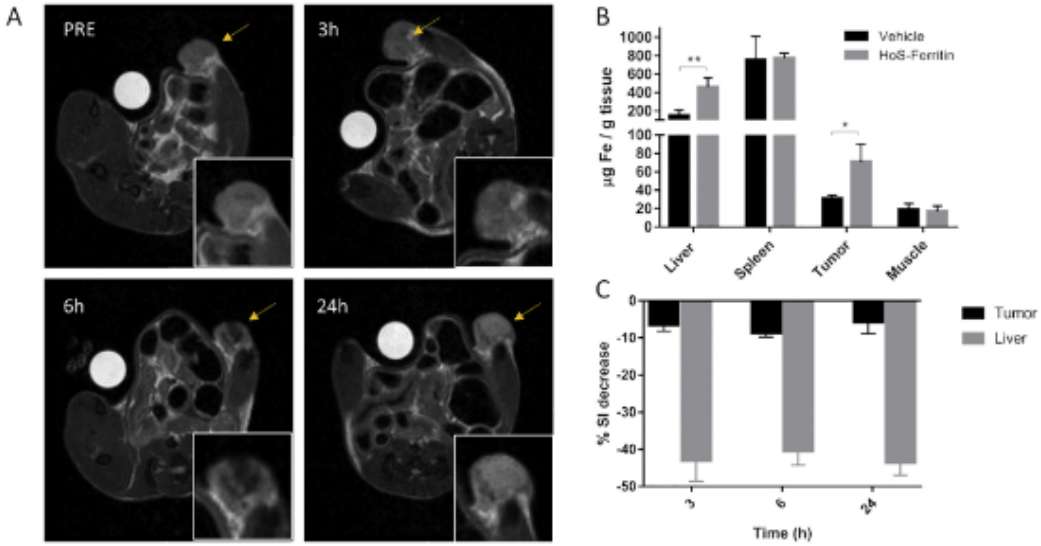

Fig. 5. (A) *In vivo* MRI on BALB/c mice inoculated with TS/A cells. T2-weighted MR images (tumor region) acquired before and 3 h, 6 h and 24 h after the administration of HoS-ferritin at a protein dose of 90 mg/kg. The arrow indicates tumor region enlarged in the bottom panel. The measured SI was normalized to a standard Gd(III) solution in an external reference tube. (B) ICP-MS analysis of iron content performed *ex vivo* 24 h after HoS-ferritin administration in liver, spleen, tumor and muscle in vehicle and HoS-ferritin treated mice. Statistical analysis 2way ANOVA, *$p < .05$, **$p < .01$. (C) Percentage of SI decrease calculated on T2-weighted MR images in tumor and liver.

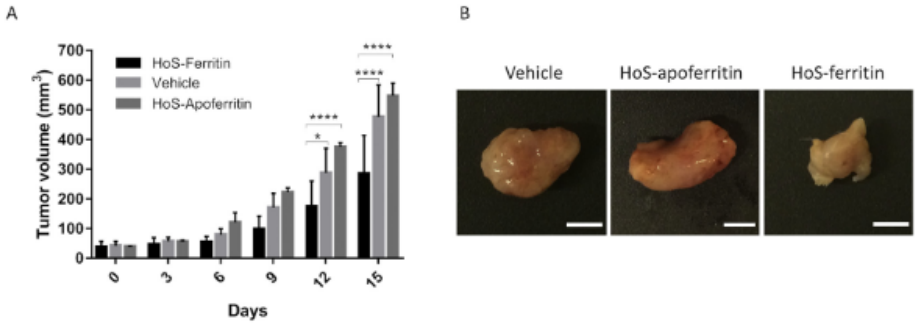

Fig. 6. (A) Tumor growth, measured by MRI, monitored every three days after the injection of HoS-ferritin (45 mg/kg), HoS-apoferritin (45 mg/kg) or vehicle (0.9% saline solution). (B) Representative pictures of TS/A inoculated tumors in BALB/c mice, obtained after explantation at the end of the treatment with HoS-ferritin, HoS-apoferritin or vehicle. Scale bars = 0.5 cm.

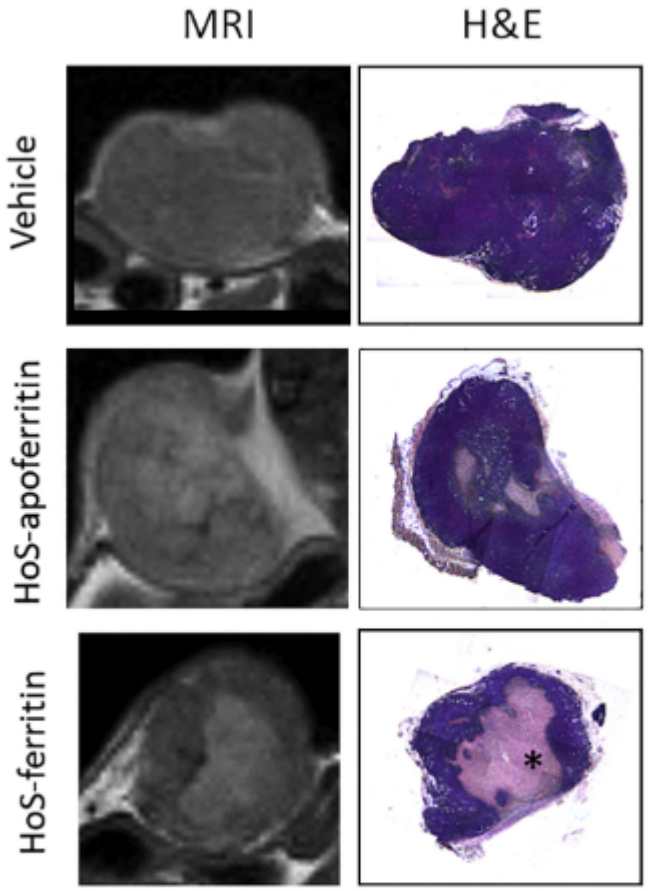

Fig. 7. Comparision between T2-weighted MRI and H&E histological images of TS/A vehicle, HoS-apoferritin and HoS-ferritin treated tumors. Asterisks indicate necrosis area. H&E images of hole tumors were reconstructed from multiple pictures (magnification × 2.5).

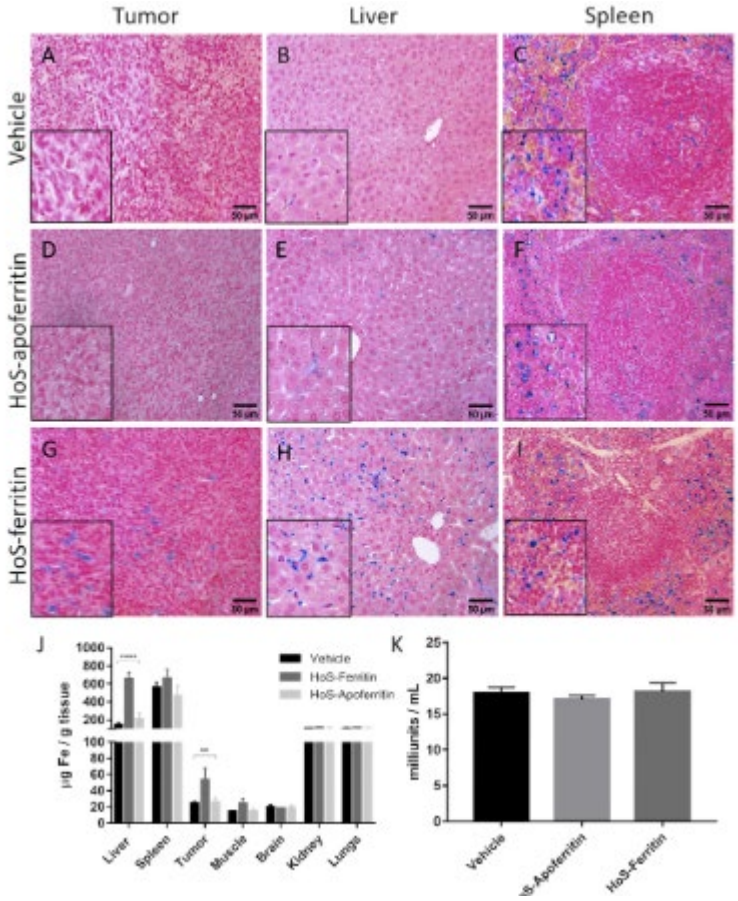
Tumor
Liver
Spleen
Vehicle
HoS-apoferritin
HoS-ferritin
A
B
C
D
E
F
G
H
I
J
K
μg Fe / g tissue
Vehicle
HoS-Ferritin
HoS-Apoferritin
Liver
Spleen
Tumor
Muscle
Brain
Kidney
Lungs
milliunits / mL
Vehicle
HoS-Ferritin